Molecular and Functional Characterization of H$_v$1 Proton Channel in Human Granulocytes

Gábor L. Petheő[1,2]*, Anna Orient[1], Mónika Baráth[3], István Kovács[1], Bence Réthi[3], Árpád Lányi[3], Anikó Rajki[1,2], Éva Rajnavölgyi[3], Miklós Geiszt[1]

1 Department of Physiology, Faculty of Medicine, Semmelweis University, Budapest, Hungary, 2 Laboratory of Neurobiochemistry and Molecular Physiology, Hungarian Academy of Sciences, Budapest, Hungary, 3 Institute of Immunology, Medical and Health Science Center, University of Debrecen, Debrecen, Hungary

Abstract

Voltage-gated proton current (I$_{Hv}$) has been characterized in several cell types, but the majority of the data was collected in phagocytes, especially in human granulocytes. The prevailing view about the role of I$_{Hv}$ in phagocytes is that it is an essential supporter of the intense and sustained activity of Nox2 (the core enzyme of the phagocyte NADPH oxidase complex) during respiratory burst. Recently H$_v$1, a voltage-gated proton channel, was cloned, and leukocytes from H$_v$1 knockout mice display impaired respiratory burst. On the other hand, hardly anything is known about H$_v$1 in human granulocytes. Using qPCR and a self made antibody, we detected a significant amount of H$_v$1 in human eosinophil and neutrophil granulocytes and in PLB-985 leukemia cells. Using different crosslinking agents and detergents in reducing and non-reducing PAGE, significant expression of H$_v$1 homodimers, but not that of higher-order multimers, could be detected in granulocytes. Results of subcellular fractionation and confocal imaging indicate that H$_v$1 is resident in both plasmalemmal and granular membrane compartments of resting neutrophils. Furthermore, it is also demonstrated that H$_v$1 accumulates in phagosome wall during zymosan engulfment together with, but independently of Nox2. During granulocytic differentiation early and parallel upregulation of H$_v$1 and Nox2 expression was observed in PLB-985 cells. The upregulation of H$_v$1 or Nox2 expression did not require the normal expression of the other molecule. Using RNA interference, we obtained strong correlation between H$_v$1 expression and I$_{Hv}$ density in PLB-985 cells. It is also demonstrated that a massive reduction in H$_v$1 expression can limit the Nox2 mediated superoxide production of PLB-985 granulocytes. In summary, beside monomers native H$_v$1 forms stable proton channel dimer in resting and activated human granulocytes. The expression pattern of H$_v$1 in granulocytes is optimized to support intense NADPH oxidase activity.

Introduction

Voltage-gated (depolarization-activated) proton current (I$_{Hv}$) has been described in a set of mammalian and non-mammalian cells. Most studies characterizing the biophysical and pharmacological properties of this current have been conducted on human cells of hemopoietic origin, such as macrophages, lymphocytes, leukemia cell lines and granulocytes (for a detailed review on I$_{Hv}$s see: Ref. [1]). The identity of the I$_{Hv}$ carrying molecule had been obscure for many years, but in 2006 two groups have cloned a novel "voltage sensor only protein" (VSOP) from mouse [2] and human [3]. Heterologous expression of the two mammalian VSOPs induced the emergence of characteristic voltage-gated proton currents in a variety of cell lines [2–4]. Based on these results the name Hydrogen Voltage-gated Channel 1 was coined, and now is widely used to refer to the genes encoding these VSOPs (HVCN1) and to their products (H$_v$1). Importantly, purified and reconstituted human H$_v$1 induced depolarization-dependent proton permeability in liposomes [5], ultimately proving that H$_v$1 can function as a depolarization-activated proton pathway. A series of publications have also demonstrated that mouse and human H$_v$1, although functional in the monomeric form, tend to form dimers in transfected cells [6–8].

Despite the extensive studies, little is known about the function of the voltage-gated proton channel in leukocytes and in other cell types [9]. In case of phagocytes the widely accepted view is that this channel is essential to blunt the potentially deleterious consequences of phagocyte NADPH oxidase (phox) activity. Upon activation the core enzyme of the phox complex Nox2 (a.k.a. gp91^{phox}) transports electrons from NADPH to molecular oxygen to produce superoxide. Superoxide anion is then converted into other, more toxic reactive oxygen species (ROS) which are involved in killing pathogens [10]. Without compensatory mechanisms the intensity of the transmembrane electron transport is high enough to generate intolerable membrane depolarization and intracellular acidification, which would eventually also block the oxidase itself [11]. Supporting the role of H$_v$1-mediated proton flux in charge compensation, it was shown recently that leukocytes from H$_v$1 knockout (H$_v$1$^{-/-}$) mice display 30 to 75% reduction in phorbol ester-induced ROS production [12–14]. Importantly, H$_v$1$^{-/-}$ cells were devoid of voltage-gated proton current [12–14], and their ROS production could be normalized by incorporating a

proton permeable, monovalent cation channel (gramicidin) into their membrane [14]. Beside the compromised oxidase activity, neutrophils from H$_v$1$^{-/-}$ mice also displayed abnormal migration and intracellular Ca^{2+} turnover [14]. It has to be noted, however, that H$_v$1$^{-/-}$ cells also produced massive amounts of ROS [12–14], and an impact of H$_v$1$^{-/-}$ genotype on leukocyte development is not yet ruled out.

Results obtained using heterologous expression systems or knockout (KO) mice, although indispensable in many respects, can provide only limited and indirect information on the expression and function of H$_v$1 in human cells. Therefore, amongst others, the following questions remain open concerning the proton channel molecule of human granulocytes: A) Is HVCN1 the gene that codes for proton channel in human granulocytes? B) Assuming that H$_v$1 is in fact the proton channel of granulocytes, is it expressed as a monomer or multimer, and does the activation with phorbol-12-myristate-13-acetate (PMA) alter the tendency of H$_v$1 to adopt these structures? C) To what cellular membranes does H$_V$1 localize in resting and in phagocytosing granulocytes? D) Do H$_v$1 and Nox2 colocalize in granulocytes? Importantly, data from patch-clamp studies indicated the codistribution of the proton channel with Nox2 in human eosinophils [15]. Furthermore, it has been advocated by different work groups that the proton channel is a built-in part of the phagocyte oxidase [16,17]. E) Is normal H$_v$1 expression required for normal expression and/or activity of Nox2?

To clarify the above uncertainties, we set out to define the main characteristics of H$_v$1 expression in human granulocytes on the cellular, subcellular and molecular level and also its relationship to Nox2. Our results indicate that H$_v$1 is expressed in intracellular membranes and on the cell surface of granulocytes. Native H$_v$1 molecule is expressed in dimer and monomer form in different leukocytes and its expression is required for normal voltage-gated proton currents in different leukemia cell lines. Additionally, H$_v$1 and Nox2 colocalize in granulocytes, and both accumulate in the same membrane compartment upon activation. Furthermore, severely impaired H$_v$1 expression can reduce the maximum rate of superoxide release in a human granulocyte cell line PLB-985.

Results

Expression of H$_v$1 in human leukocytes

We used two approaches to verify the expression of H$_v$1 in human leukocytes. To assess the mRNA level, quantitative real time PCR assays (qPCR) were performed. To detect the expression of the H$_v$1 protein, total cell lysates were prepared from different human blood cells. Because of their limited availability, we did not attempt to perform the experiments on basophil granulocytes and natural killer cells. We have raised an affinity purified, polyclonal antibody (aH$_v$1-N) that selectively recognizes the intracellular N-terminal domain of the human H$_v$1 protein in Western blots (WB) and immunofluorescence experiments (see Materiala and Methods and Fig. S1 for details). As it is demonstrated on Figs. 1a and 1b, both qPCR and WB indicated that all tested leukocyte subsets except T-cells express significant amount of H$_v$1 mRNA and display significant aH$_v$1-N labeling around 30 kDa. This result is in agreement with reports on the density of voltage-gated proton current in human leukocytes [1]. Similar to T-cells, membrane sample of erythrocytes lacked significant aH$_v$1-N labeling in WB (not shown).

H$_v$1 forms stable dimers in human granulocytes

An interesting outcome of the WB experiment was that each of the phagocytic cell types displayed faint aH$_v$1-N labeling at
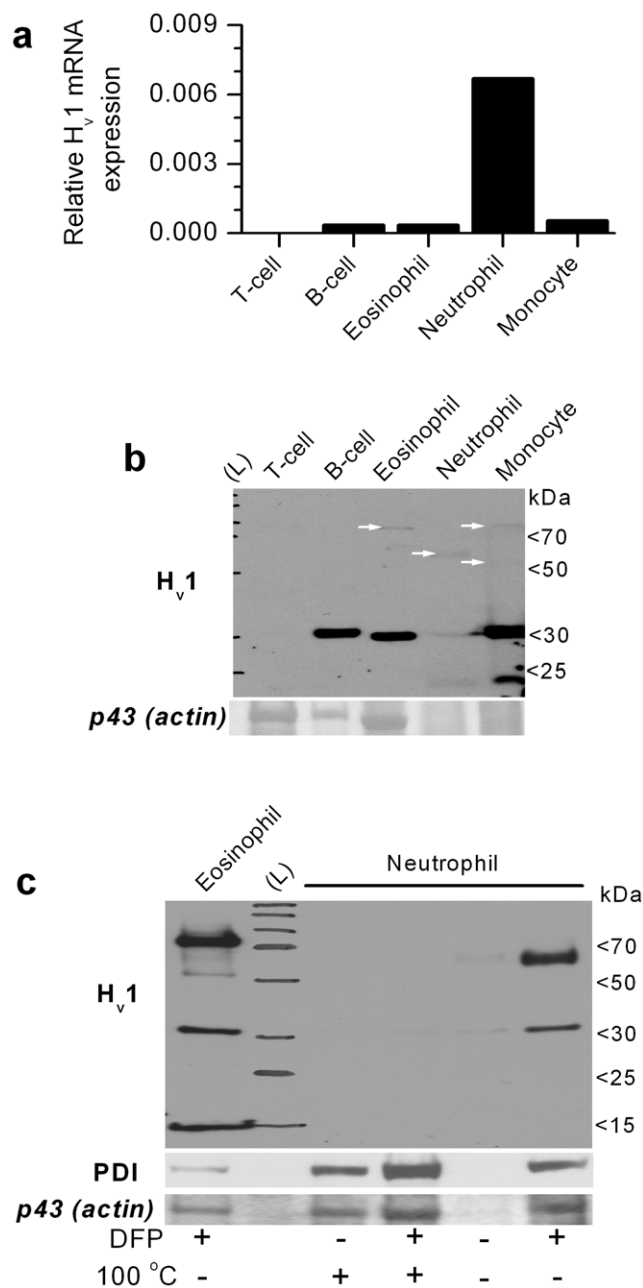

Figure 1. Expression pattern of H$_v$1 mRNA and protein in major classes of human peripheral blood leukocytes. (a) Real-time qPCR analysis of H$_v$1 mRNA expression relative to cyclophilin mRNA level (similar relative expressions were observed if genes other than cyclophilin were used for normalization). Data represent the mean result of a duplicate experiment. The experiment was repeated in an independent set of leukocytes with similar results. **(b)** Western blot analysis of H$_v$1 expression in the same cell types as detected with aH$_v$1-N. Total cell lysates of 10^6 cells were loaded each lane. The lane with stained molecular weight marker is labeled with (L). Ponceau-stained ~43 kDa apparent M$_w$ protein band (putative actin) demonstrates the protein load and the quality of the samples. The absence of clear actin band in the neutrophil and monocyte lanes indicates massive protein degradation. Note that immunolabeling of proteins which are considered "house keeping" (e.g. actin or PDI) is of very limited use in case of cell types with very different proteolytic activity, motility and metabolism. Importantly, aH$_v$1-N also detects one or more faint band between ~60 and ~80 kDa in myeloid cell types (white arrows). **(c)** Detection of H$_v$1 and higher M$_w$ bands is hampered in granulocytes by serine proteases and sample heat treatment. Total cell lysates of 5×10^5

cells were loaded each lane. Ponceau-stained ~43 kDa apparent M$_w$ protein band (putative actin) and aPDI labeling demonstrate the degree of protein degradation. Note that anti-PDI signal and the intensity of the actin band is well correlated, which justifies the use of the latter signal to demonstrate protein load and sample quality. DFP incubation for 30 min on ice before cell lysis and heating of the sample (at 100°C for 10 min) were applied as indicated. This experiment was designed based on results from pilot studies, and was performed for demonstration purposes only, thus it was not repeated in this form. In diverse experiments low M$_w$ H$_v$1 labeling was occasionally observed after DFP treatment, which was independent of the granulocyte type, and likely reflects some remaining protease activity in the given sample. doi:10.1371/journal.pone.0014081.g001

molecular weights significantly higher than 30 kDa, typically between 60 and 80 kDa. Furthermore, in neutrophils and monocytes a lower M$_w$ band was also present. We assumed that the variability in the labeling pattern could arise from the presence of H$_v$1 dimers (as described in heterologous expression systems [6–8]) and from proteolytic degradation of H$_v$1. Granulocytes, especially neutrophils, express high amounts of various proteases, which may explain the discrepancy between the low H$_v$1 protein signal and high mRNA expression level. Therefore, in follow-up experiments we attempted to improve the detection of H$_v$1 and its putative dimer in granulocytes. Fig. 1c demonstrates that heat exposure and the action of DFP-sensitive serine proteases reduce the amount of detectable monomeric and high M$_w$ H$_v$1 forms. The detrimental effect of serine proteases could be reasonably evaded if the membrane permeable protease inhibitor DFP had been added to granulocytes before cell lysis (see Material and Methods for details). The remaining low M$_w$ labeling (e.g. in the eosinophil sample in this experiment) indicates that H$_v$1 degradation could not be completely prevented. Interestingly, the dominant high M$_w$ band migrated with different speeds in case of eosinophils and neutrophils in this experiment. Upon repeated testing, however, no correlation between granulocyte type and migration velocity of the putative dimer could be established. Additionally, a double band around 70 kDa was observed sometimes. It is unlikely that one of the high M$_w$ bands arises from a H$_v$1 bound accessory protein, since Koch et al. observed similar double band migration of the heterologously overexpressed mouse H$_v$1 dimer in non-reducing PAGE [8]. Therefore, we assume that the H$_v$1 dimer can migrate at least in two different stable conformations.

To further explore the interactions between monomers, granulocyte cell lysates were prepared using 2x Laemmli sample buffers with modified detergent compositions, and with or without the addition of the reducing agent β-mercaptoethanol (β-ME). To minimize the re-oxidation of the sample due to β-ME decomposition, it was added shortly (~15 min) before starting the PAGE. Results in Fig. 2a indicate that the presence of β-ME and high concentration of ionic detergent (SDS) favors the detection of the H$_v$1 monomer. Using mainly non-ionic detergent (Tween20) during sample preparation, the dimer form is prevailing, which migrates in two major bands under non-reducing conditions. The above data strongly indicate that H$_v$1 dimers are present natively in human granulocytes and that both strong polar interactions and disulfide formation are capable for stabilizing the dimer upon solubilization.

The use of non-ionic detergent is advantageous for preserving native protein-protein interactions, e.g. to confirm the natural presence of such interactions between H$_v$1 monomers. On the other hand, low SDS concentration may not denature proteases and may not provide sufficient negative charge to proteins. These drawbacks result in fainter and less clear bands in Western blot
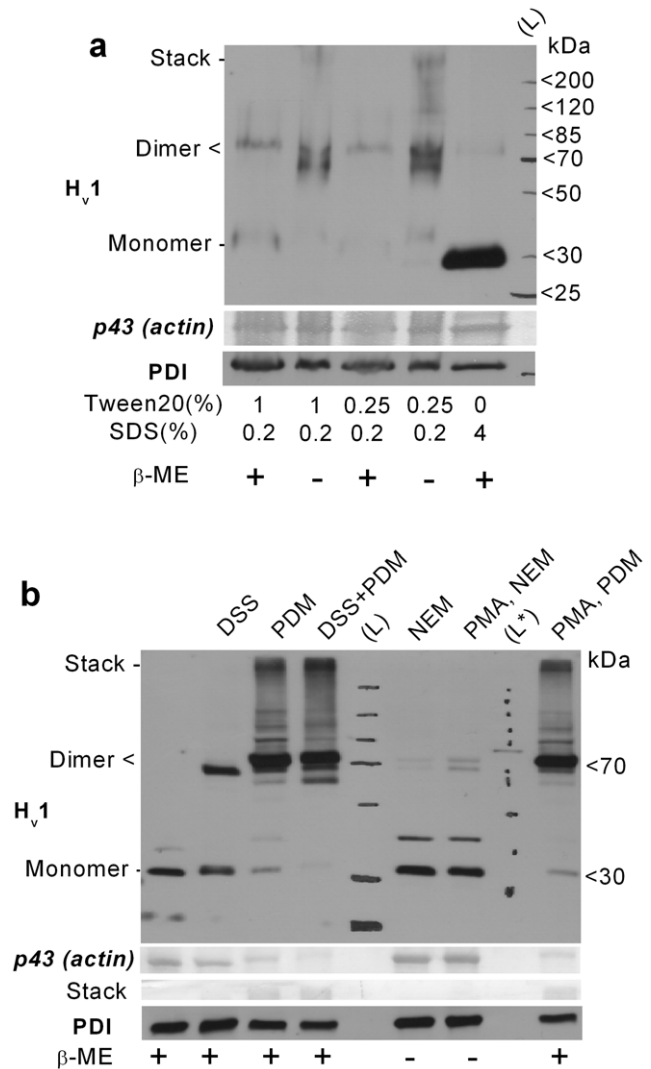

Figure 2. H$_v$1 dimers are natively present in human granulocytes. (a) Total cell lysates of 10^6 PMNs were loaded each lane. DFP-treated cells were lysed in modified 2x Laemmli sample buffer supplemented with 2 mM PMSF. Detergent composition and the presence of 5% v/v β-mercaptoethanol in the sample buffer are indicated below. **(b)** WB detection of H$_v$1 dimers in granulocyte samples treated with amino- (DSS) or thiol-reactive (PDM) crosslinkers or with thiol-reactive alkylating agent (NEM). The increase in labeling with aH$_v$1-N at ~70 kDa is at the expense of that at ~30 kDa in cross-linked samples. The appearance of higher (above 75 kDa) M$_w$ aH$_v$1-N-labeled bands is likely, at least in part, due to crosslinking of H$_v$1 with other proteins. PMA pretreatment (200 nM for 15 min) exerted only minor effect on the vicinal cysteines in the H$_v$1 dimer. The identity of the faint, ~40 kDa band is not clear, and it was not consistently detected. Ponceau-stained ~43 kDa band (putative actin) and near stack region demonstrates the protein load and sample crosslinking. The presence of 5% v/v β-mercaptoethanol in the sample buffer is indicated below. L* denotes unstained M$_w$ marker used for calibrating the routinely used, stained M$_w$ marker.
doi:10.1371/journal.pone.0014081.g002

experiments, due to protein degradation and less uniform migration velocity. Therefore, in follow-up experiments we attempted to stabilize native dimers using crosslinking agents to detect them in standard SDS-PAGE. The amino group-specific bifunctional crosslinker disuccinimidyl suberate (DSS) was earlier used by two groups to improve the detection of H$_v$1 dimers in H$_v$1

transfected cell lines [7,8]. Treating granulocytes with DSS before cell lysis, efficiently increased the detection of the dimeric H$_v$1 form in standard reducing PAGE (Fig. 2b). Additionally, the presence of H$_v$1 homodimers in all major types of human leukocytes and in differentiated PLB-985 granulocytes could be confirmed using DSS (Fig. S2b). Because monomeric and dimeric H$_v$1 forms support kinetically different voltage-gated proton currents [8], it was suggested that the transition between the two forms could lead to some of the proton current phenotype changes observed in granulocytes during phox activation. [14]. Importantly, however, pretreating cells with a supramaximal phox activating dose of PMA (200 nM for 15 min) before DSS addition did not alter its crosslinking potential in granulocytes or in differentiated PLB-985 cells (data not shown).

Although H$_v$1 dimers do not seem to decompose upon cell activation, disulfide formation has been reported to participate in redox regulation of different ion channels [18]. We used N-ethylmaleimide (NEM) and N,N'-(1,3-phenylene)dimaleimide (PDM) to explore the possible influence of redox changes during the PMA-induced oxidative burst on disulfide formation. Both NEM and PDM react covalently with reduced cysteine residues, but while PDM is a homobifunctional crosslinker and mimics disulfide formation, NEM prevents it. To get a snapshot on the redox state of the cysteines possibly involved in H$_v$1 dimerization, the thiol reactive compounds were added after the cells were placed on ice. PDM could drive dimer formation near to completion during the 40 min incubation. On the other hand, NEM almost completely prevented the detection of the dimer independently of PMA preactivation (Fig. 2b). These results indicate that although certain cysteines in the apposed H$_v$1 monomers become vicinal, they are mainly in reduced state. Massive oxidation of the apposed cysteines is unlikely even in PMA-activated cells, as the action of PDM and NEM on dimer formation was hardly affected by PMA treatment. Importantly, PMA treatment did not alter the amount of H$_v$1 protein in granulocytes. The detected H$_v$1 density in WBs from PMA-treated samples was $96\pm10\%$ (n = 5) of that from resting cells.

It is theoretically possible that not monomer and dimer, but a higher-order multimer is the dominant native confirmation of H$_v$1 in granulocytes. We reasoned that we should be able to detect such multimers as clear and dominant band if we apply more intense crosslinking (DSS + PDM for 1 h) or if we solubilize cells with non-ionic detergent after DSS crosslinking. In all cases, however, massive labeling was detected only around 70 kDa and in the stacking region, even if monomers became completely undetectable (data not shown). Labeling in the stacking region may result form non-specific interactions and/or network like crosslinking of macromolecular complexes. Therefore, if higher-order multimers are present in granulocytes their occurrence is much less likely than that of dimers or interactions with other proteins.

H$_v$1 primarily localizes to intracellular membranes in granulocytes

Data on the subcellular distribution of native H$_v$1 in human granulocytes is lacking, but a recent study demonstrates that the heterologously overexpressed H$_v$1 locates to intracellular membrane compartments in HeLa cells [19]. The accumulation of H$_v$1 in phagosome membrane in mouse granulocytes [12] and in late endosomes of human lymphocytes [20] was also demonstrated. To explore the subcellular distribution of H$_v$1 in human granulocytes, purified, adherent granulocytes, adherent PLB-985 granulocytes and smears of whole blood were labeled with aH$_v$1-N along with the monoclonal anti-Nox2 antibody 7D5 [21]. Nox2 labeling was routinely applied to see whether the strong functional coupling

between Nox2 and the voltage-gated proton channel [11] is mirrored in their distribution. Another rationale of 7D5 colabeling is that the localization of Nox2 in granulocytes is relatively well explored [22,23]. Distribution of H$_v$1 and Nox2 was detected using confocal laser scanning microscopy. Eosinophils displayed strong labeling with aH$_v$1-N, while neutrophils generally were labeled weaker but with variable intensity (Fig. 3a). Differentiated PLB-985 cells also displayed significant labeling for H$_v$1. Subcellular colocalization of H$_v$1 and Nox2 was a general finding. The lowest correlation in the two signal intensities was detected in neutrophils. Pearson's coefficients for neutrophils, eosinophils and differentiated PLB-985 cells were 0.68 ± 0.03 (n = 5) 0.84 ± 0.03 (n = 5), and 0.92 ± 0.03 (n = 4), respectively. The moderate correlation in the two signal intensities in neutrophils, as compared to the other leukocyte types, was surprising. Therefore, the analysis was repeated in DFP-pretreated neutrophils (Fig. 3a) to inhibit serine proteases and apoptosis [24]. Under these conditions Pearson's coefficients increased to 0.78 ± 0.2 (n = 8, $p<0.05$, Kolgomrov-Smirnov test). This result indicates that proteolytic degradation can spoil the detection of H$_v$1 also in immunofluorescence experiments, resulting in the underestimation of H$_v$1 and Nox2 colocalization. Among granulocytes PLB-985 cells displayed the most pronounced granular pattern, but in none of the tested leukocyte types localized H$_v$1 dominantly to the cell surface. Weak or no signal was present over the nucleus in mature cells (the results obtained on mononuclear cells are available as Fig. S2a).

To verify the results obtained with confocal microscopy, WBs were performed on subcellular fractions of resting neutrophils. Confirming the results from confocal slices, significant H$_v$1 signal could be detected in fractions of both granule (β_1 and β_2) and plasma membrane origin (γ, Fig. 3). The distribution of H$_v$1 and Nox2 among the different fractions was similar, although not strictly correlated. Azurophil (α) granules, that are practically devoid of Nox2 [22], sometimes displayed marginal labeling for H$_v$1 (not shown). In case of eosinophils, the strong colocalization with Nox2 suggests that H$_v$1 localizes to the plasma membrane and to the membrane of small granules [23].

Phagocytosis induces H$_v$1 clustering

The prevailing view about the role of proton channel in phagocytes is that the channel is essential for the sustained activity of the phox during respiratory burst, mainly to provide compensatory charge for the depolarizing electron flow [9]. For such a task, proton channels should locate to the membrane compartment of intense electron transport, i.e. to the site of oxidase assembly and activity. Phagocyte NADPH oxidase promotes the antimicrobial activity of the phagosome during pathogen elimination [25], and assembly of phox subunits at the site of phagocytosis have been demonstrated [26,27]. To explore whether H$_v$1 is present on phagosomes, phagocytosis was induced by the addition of serum opsonized zymosan to purified, adherent granulocytes (more than 90% neutrophils) and to PLB-985 cells differentiated into granulcyte like cells. After 10 min the formation of phagocytic cups and closed phagosomes could be detected. Intense 7D5 labeling around engulfed zymosan particles indicated the accumulation of Nox2 in the phagosomal membrane (Fig. 4). Often overlapping with the 7D5 signal, the accumulation of aH$_v$1-N labeling in zymosan surrounding areas was also pronounced in both cell types. The phagosomal accumulation of H$_v$1 does not appear to require a functional oxidase, because strong clustering of the aH$_v$1-N signal could also be detected in differentiated PLB-985 X CGD cells, a PLB-985 clone in which Nox2 is absent (i.e. the mutant, ~56 kDa Nox2 gene product is not functional and is readily degraded) [28].
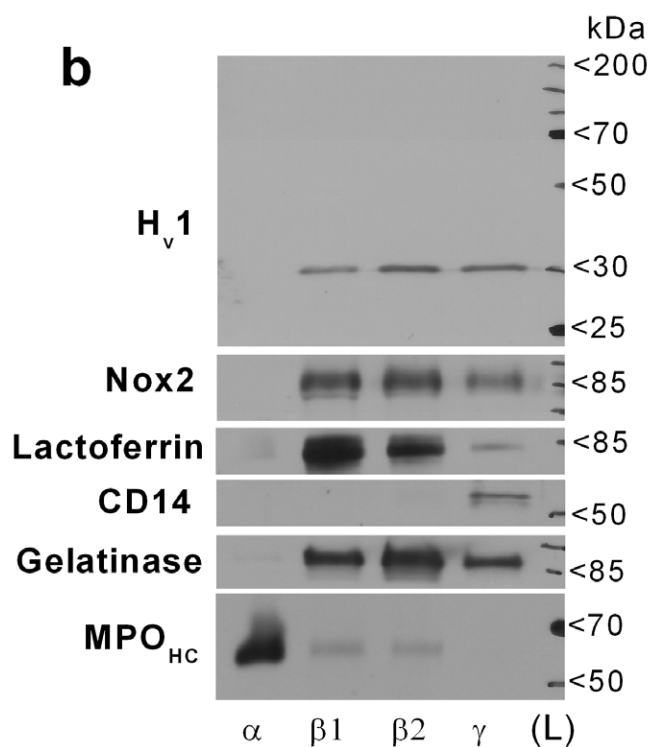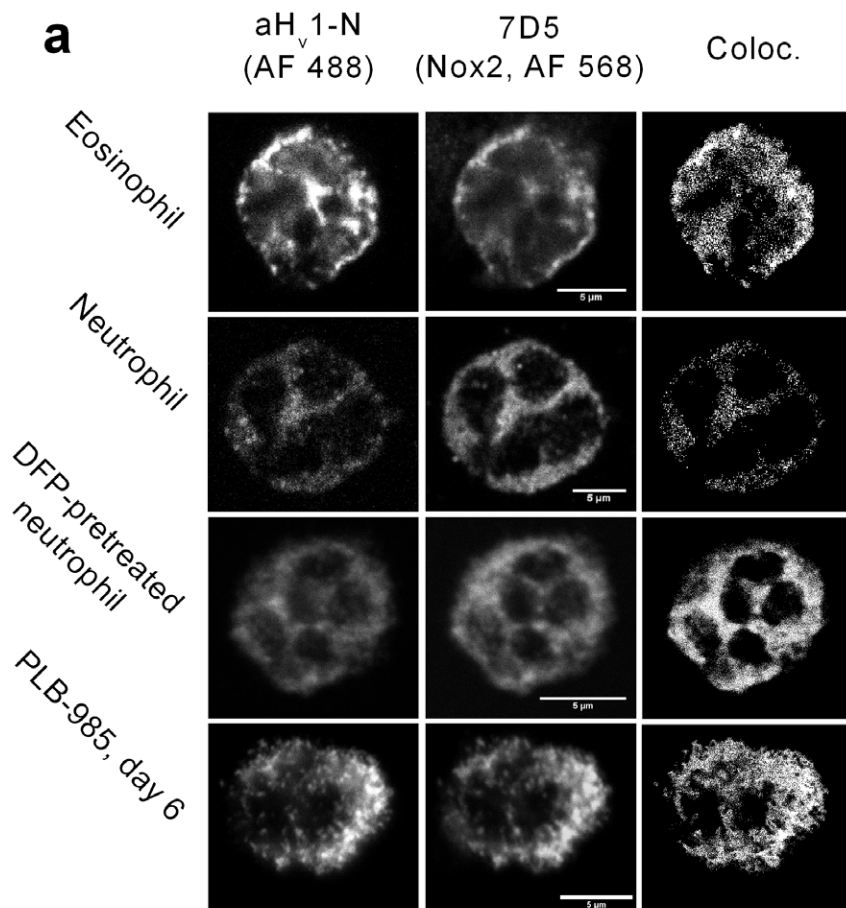
Figure 3. Partial colocalization of H$_v$1 and Nox2 in different types of human granulocytes. (**a**) Detection of H$_v$1 (left-most column) and Nox2 (middle) in granulocytes. (Scale bars represent 5 μm). Pretreating neutrophils with DFP improved the detection of H$_v$1. Colocalization analysis

was performed only in cells, in which above-threshold labeling (two times above background, see below) for both proteins could be detected. Colocalizing pixels are displayed as white dots in the most right column. Negligible Alexa Fluor® signals (considered as background) were detected with control primary antibodies (not shown). (**b**) Western blot analysis of the distribution of H$_v$1 and Nox2 between granule fractions of resting neutrophils after standard reducing PAGE. Ponceau stain confirmed that similar protein amount was loaded each lane (not shown). The different fractions are: azurophil (α), specific (β_1), gelatinase (β_2) granules and secretory vesicle together with plasma membrane (γ). Immunodetection of lactoferrin, gelatinase, CD14 and the heavy chain of myeloperoxidase (MPO$_{HC}$) demonstrates the purity of the membrane preparates [22].
doi:10.1371/journal.pone.0014081.g003

H$_v$1 expression and proton current density are correlated in PLB-985 cells

Leukocytes from H$_v$1 knockout mice lack voltage-gated proton currents, indicating that H$_v$1 is essential for these currents in the mouse [12–14]. A similar genetical model is not available in human, as no inherited H$_v$1 deficiency has been reported. Therefore, an ultimate proof is lacking to qualify H$_v$1 as the proton channel molecule of human leukocytes. To investigate the
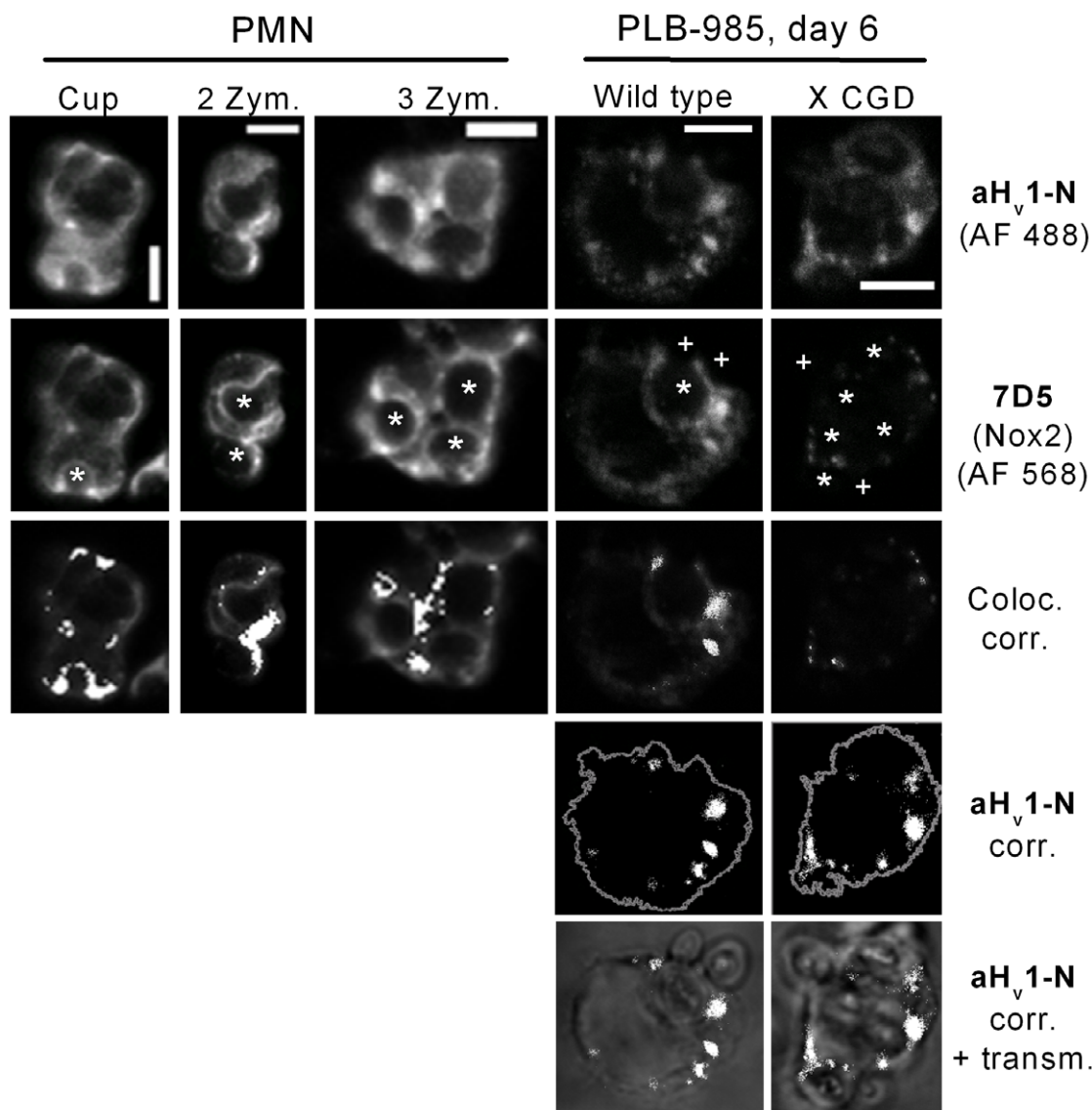

Figure 4. Partial intracellular colocalization of H$_v$1 and Nox2 in phagocytosing granulocytes. H$_v$1 (first raw) and Nox2 (second raw) tend to cluster during Zymosan phagocytosis, as detected in immunofluorescence experiments using confocal laser microscopy. The locations of zymosans are indicated by white asterisks. Forming (phagocytic cup, first column) and closed phagosomes (second and third column) are visible as round, hollow structures. In further analyses only pixels with intensity at least two times the average intensity (threshold) observed in experiments with control antibodies were included (activated phagocytes displayed significant, diffuse labeling in control experiments, not shown). Clusters of H$_v$1 and Nox2 are often colocalized (third row). Colocalizing pixels are superimposed as white dots on the dimmed picture of 7D5 labeling (scale bars represent 5 µm). H$_v$1 clustering is independent of Nox2 in PLB-985 cells (fourth raw). Cell perimeter (as derived form background labeling with H$_v$1) is outlined in gray, and above-threshold H$_v$1 labeling is presented as white dots. In the fifth raw above-threshold H$_v$1 signals are superimposed as white dots over the (dimmed) visible light transmission image of phagocytosing cells. Pseudo color, 3D reconstructions of the cells in the 3rd and 4th columns are provided as supplemental Videos S1 and S2, respectively.
doi:10.1371/journal.pone.0014081.g004

putative proton channel role of H$_v$1 in human leukocytes, three small interfering RNAs (siRNAs) were designed corresponding to sequences only present in the H$_v$1 mRNA. Of the three siRNAs two (si-1 and si-2) efficiently knocked down H$_v$1 expression in transfected COS-7 cells (not shown), as compared to their minimally altered control sequences (si-1c and si-2c). Of the two effective constructs only the si-2/-2c pair proved to be non-toxic in long-term cell culture experiments. To establish the relationship between H$_v$1 level and proton current density in a human myeloid leukemia cell line, PLB-985 cells were stably transfected with plasmids containing puromycin resistance gene and a short hairpin RNA (shRNA) sequence encoding either si-2 or si-2c. After the analysis of H$_v$1 protein expression in puromycin-resistant PLB-985 clones, three control and two H$_v$1 knock-down clones were tested in whole-cell patch-clamp experiments (Fig. 5a). The results indicate that the density of characteristic voltage-gated proton currents and the H$_v$1 expression level is well correlated in non-differentiated PLB-985 clones (Fig. 5b). Furthermore, the expression of the same shRNAs in a lymphoid leukemia cell line (Jurkat) also resulted in the reduction of proton current density (Fig. S3). These data support the view that H$_v$1 is indispensable for voltage-gated proton currents in human leukocytes.

H$_v$1 and Nox2 expression is upregulated in parallel during granulocytic differentiation

During granulocytic differentiation of human HL-60 leukemia cells the occurrence and development of proton conductance is paralleled by the functional and biochemical appearance of the phox [29]. We were interested whether the expression of the two proteins is by any means correlated during granulocytic differentiation. In PLB-985 cells, a subclone of HL-60 cells [30], the level of phox components also increases upon granulocytic differentiation [28]. We decided to use PLB-985 cells to study the relationship between H$_v$1 and Nox2 expression, since a Nox2 gene-disrupted clone is also available (PLB-985 X CGD [28]). The expression level of both H$_v$1 and Nox2 gradually increased after inducing differentiation with DMFA (Fig. 6a). The change in the amount of both proteins was most pronounced during the first two days. To test whether this parallel change in protein level reflects an interdependence of H$_v$1 and Nox2 expression, the experiment was repeated in Nox2 deficient (X CGD) PLB-985 cells. Each tested day after starting the DMFA-induced differentiation the H$_v$1 expression appeared reduced in Nox2 deficient cells (Fig. 6a). The difference in aH$_v$1-N labeling of the two cell lines after 6-day long DMFA induction was also detected in immunofluorescence experiments (not shown). H$_v$1 expression might be impaired in PLB-985 X CGD cells for the following reasons: a) PLB-985 X CGD clone has a general differentiation problem, b) PLB-985 X CGD is a clone in which H$_v$1 expression is diminished in a Nox2 independent manner or c) normal Nox2 expression is required for normal H$_v$1 expression. The latter does not seem to be a key factor, because no major difference in the H$_v$1 level could be observed on day 7, if the differentiation pressure was increased by reducing the serum content of the culture medium (from 10 to 0.5% v/v [31], Fig. 6a).

The fact that the lack of functional phox does not have a dramatic impact on H$_v$1 expression does not rule out that normal expression of phox subunits requires normal H$_v$1 levels. To test the latter possibility, PLB-985 cell clones that express normal or diminished amounts of H$_v$1 were differentiated for 7 days in DMFA containing, low-serum medium. As Fig. 6b demonstrates,
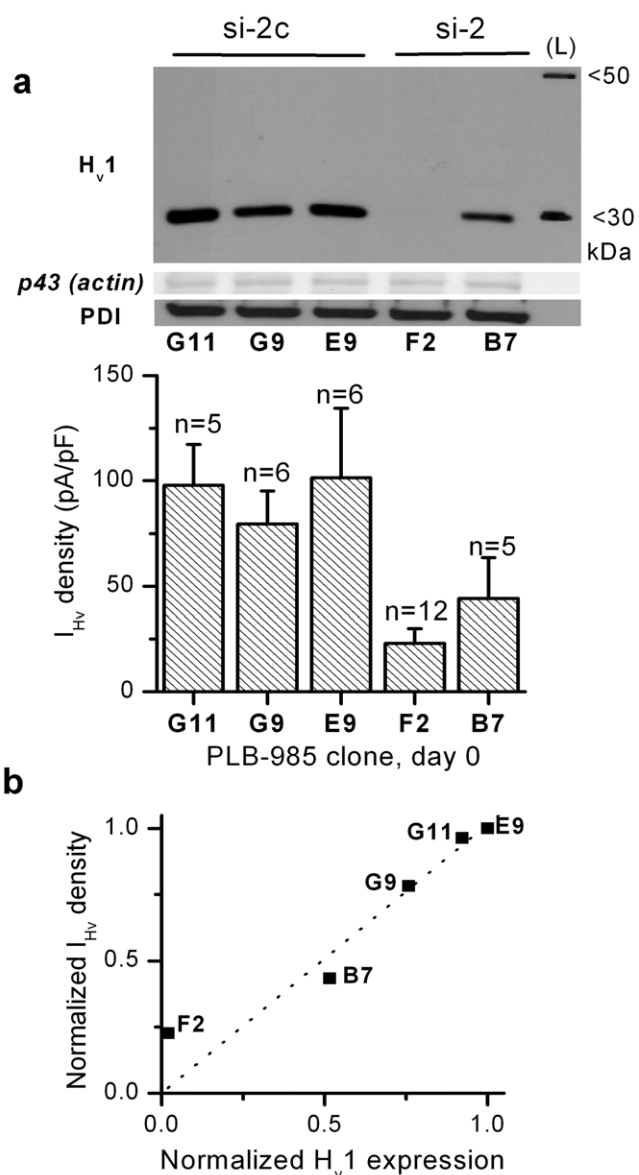

Figure 5. Correlation between H$_v$1 and voltage-gated proton current. (**a**) The expression level of H$_v$1 (top) and the corresponding I$_{Hv}$ density (below) is presented in selected PLB-985 clones. The clones were transfected with a plasmid producing siRNA capable of knocking down H$_v$1 expression (si-2) or its control siRNA (si-2c). For WB total cell lysates of 10^6 cells were loaded each lane. The I$_{Hv}$ density in clone F2 is significantly smaller than in E9 and G11 ($p < 0.05$, Kruskal-Wallis test) (**b**) Mean I$_{Hv}$ density value is plotted against the corresponding H$_v$1 signal normalized to p43 signal, as measured with densitometry. The values of each clone are divided by the values of clone E9. Dotted line is the result of linear fit constrained to path through the origin (R$>$0.97, $p<0.005$).
doi:10.1371/journal.pone.0014081.g005

massive reduction in H$_v$1 level does not prevent high-level expression of the phox subunits Nox2, p22^{phox} and p47^{phox}.

Reduced expression of H$_v$1 can limit superoxide production

The rate of ROS production is significantly reduced in leukocytes from H$_v$1 knockout mice [12–14]. Supposing that the role of H$_v$1 is the same in mouse and human leukocytes, one
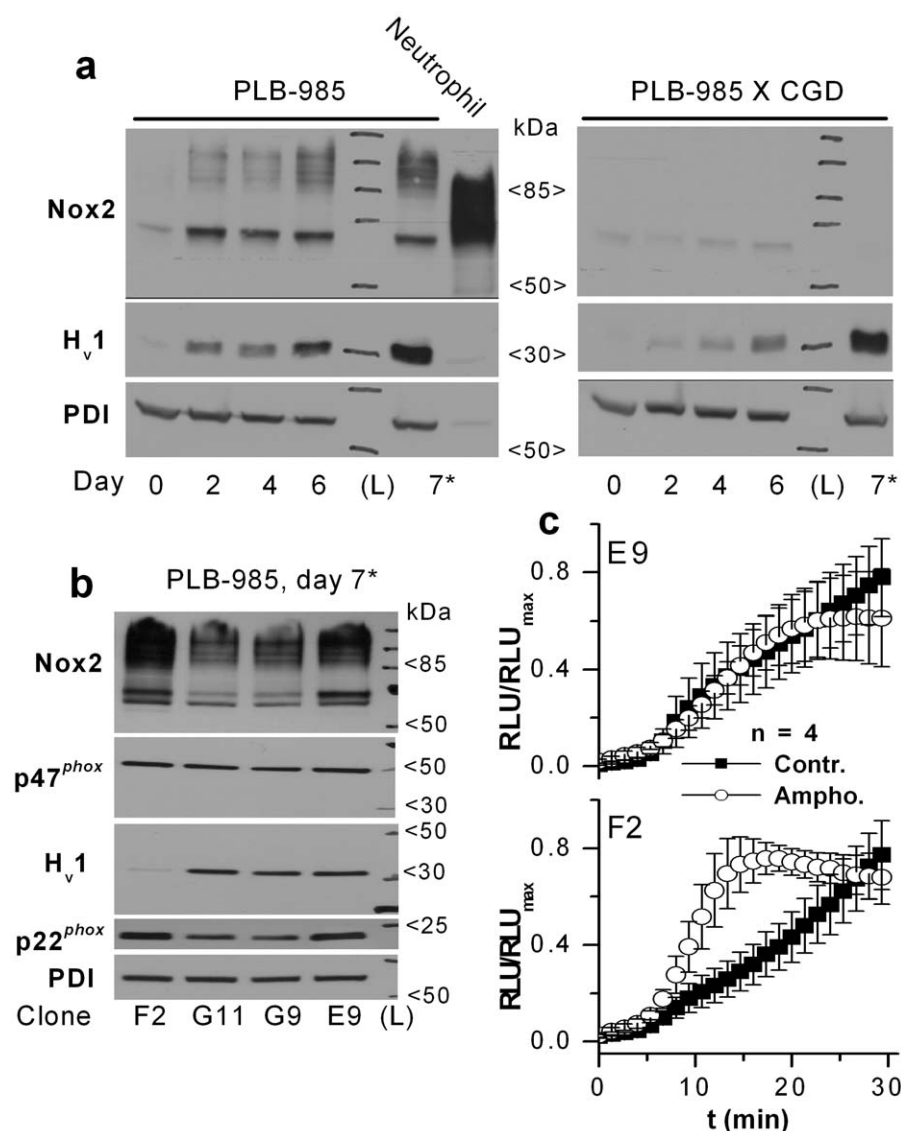
Figure 6. The functionally coupled H$_v$1 and Nox2 are induced in parallel, but largely independently during granulocytic differentiation in PLB-985 cells. (**a**) Normal H$_v$1 expression can be induced in the absence of normal Nox2 level. For WB total cell lysates of 10^6 cells were loaded each lane. Samples of PLB-985 cells were prepared before (0) and 2, 4, 6 days after inducing differentiation with 0.5% DMFA. In a separate sample (7*) cells were differentiated for 7 days, and DMFA treatment was applied in low-serum culture medium (0.5% v/v) to increase the differentiation pressure. Different anti-Nox2 labeled bands correspond to different glycozilation states of the 65 kDa Nox2 protein. (**b**) The normal expression of different phox subunits (Nox2, p22^{phox} and p47^{phox}) is not disturbed by strongly reduced H$_v$1 expression in differentiated PLB-985 cells. (**c**) Amongst differentiated PLB-985 clones amphotericin B amplifies superoxide production (2.92±0.48 times at 15 min, p<0.05, Mann-Whitney U test) only in clone F2, in which H$_v$1 expression is strongly diminished. No significant change in superoxide production was detected in E9, G9 and B7 clones in the presence of amphotericin B. Diogenes™ reagent was used to detect the extracellular release of superoxide. Cells were preincubated for 15 min in a 1:1 mixture of Diogenes™ and H-medium with or without 10 µg/ml amphotericin B. At time point 0 cells were activated by 200 nM PMA. Negligible Diogenes™ luminescence could be detected in PMA-treated, non-differentiated PLB-985 clones and during the preincubation period (not shown).
doi:10.1371/journal.pone.0014081.g006

should observe reduced ROS production in cells that display decreased H$_v$1 expression. Surprisingly, however, in pilot experiments the PMA-induced superoxide production of the H$_v$1 knock-down F2 and B7 PLB-985 clones exceeded that of G9 and G11 control clones, and was only inferior to that of clone E9 (not shown). We suspected that this result might be explained by the large heterogeneity in the Nox2 expression level of PLB-985 clones (Fig. 6b). The PMA-induced ROS production of H$_v$1$^{-/-}$ mouse granulocytes was reported to be normalized by incorporating monovalent cation channels (gramicidin peptides [32]) into their

cell membrane [14]. Although the conductances for the monovalent cations through gramicidin channels are ranked in the same order as their aqueous mobilities (i.e. proton moves fastest [32]), it is unlikely that significant proton extrusion through gramicidin was possible in the presence of normal intracellular K$^+$ concentration. This indicates that charge compensation, rather than proton removal, became the bottleneck for ROS production in PMA-activated H$_v$1 deficient cells. If the superoxide production of a differentiated PLB-985 clone in which H$_v$1 expression is knocked-down is also limited by shortage of compensatory charge

flow, we should be able to compensate for it using an artificial conductance. Therefore, we measured the PMA-induced extra-cellular superoxide release of two control (E9, G9) and two Hv1 knock-down (F2, B7) clones with or without preincubation with the ion channel forming antibiotic amphotericin B. In the presence of amphotericin B only F2 clone displayed significant increase in PMA-induced superoxide production, and only in its early phase (Fig. 6c). Superoxide production declined after ~20 min in the presence of Amphotericin B, an effect which was not specific for clone F2. As clone F2 express high level of Nox2 but very few Hv1, the above results support the notion that charge movement through Hv1 can become rate-limiting for very intense ROS production in human cells.

Discussion

A decade-long debate about the identity of the voltage-gated proton channel molecule came to an end when Hv1 (from human [3] and mouse [2]) was cloned in 2006. Many publications since have investigated the expression, structure and possible role of Hv1 in heterologous expression systems and in mouse leukocytes. On the other hand, data on Hv1 in human leukocytes [20], especially in granulocytes, are scarce. This study was aimed to define the main characteristics of Hv1 in human granulocytes.

Hv1 supports voltage-gated proton current in human leukocytes

It has been taken for granted that Hv1 is the proton channel molecule in human leukocytes, but it has never been formally demonstrated. Now we have found that the expression levels of Hv1 in major types of human blood leukocytes (Fig. 1) correspond well to proton current density data obtained in these cells. T-cells display only tiny proton currents (0.9 pA/pF [1]) and the expression of Hv1 mRNA and protein in these cells, if any, is below the reliably detectable level. In B-cells and granulocytes the abundant expression of Hv1 protein is in accordance with their pronounced proton current amplitudes (~17–200 pA/pF [1]). Peripheral blood monocytes also display remarkable Hv1 expression, but electrophysiological data is not available about voltage-gated proton currents in this cell type. Nevertheless, the presence of such currents in macrophages and in THP-1 monocyte like leukemia cell line has been extensively demonstrated [1]. In line with the above data, in our experiments knocking down Hv1 expression in leukemia cell lines PLB-985 and Jurkat, resulted in reduced I_{Hv} density (Figs. 5 and S3, respectively). Taken together, the available data strongly support the notion that Hv1 expression is essential for voltage-gated proton currents in human leukocytes.

Hv1 is capable of forming stable dimers in human granulocytes

The dimeric nature of Hv1 had been extensively investigated and characterized in heterologous expression systems [6–8]. Available results indicate the role of the C- [7,8,19] and N-terminal [6,8] intracellular domains and of the extracellular loop between S1-S2 transmembrane helices [7] in dimerization. Importantly, monomers and dimers of Hv1 give rise to kinetically distinct I_{Hv}s. Monomeric Hv1 activates faster upon depolarization [8], while subunits in the dimer display cooperative behavior [33]. Based on the above results, it was suggested that the differences in I_{Hv} kinetics of different cell types and of resting and activated phagocytes might be explained by differences in the dimer to monomer ratio of Hv1. Now we have demonstrated for the first time that in case of endogenously expressed Hv1, the dimer form is also abundantly present in all major types of human leukocytes

and in differentiated PLB-985 cells (Figs. 2 and S2b). The existence of distant dimerization sites (see above) could theoretically allow the formation of higher-order Hv1 multimers (e.g. tri- or tetramers) as well, supposing that Hv1 density is high enough in the membrane. However, in spite of various attempts, we could not prove significant formation of such multimers in human granulocytes.

The Hv1 dimer is stabilized, at least in part, by strong polar interactions in granulocytes, because high concentration of ionic detergent (4% SDS) was required to efficiently disrupt them (Fig. 2a). On the other hand, disulfide formation between monomers appears to be a minor contributor of dimer stabilization. The human Hv1 contains only two cysteines, of which cys249 in the C-terminal intracellular domain is positioned so that it is amenable to dimer stabilization [7,19]. Similar to the data obtained with heterologously expressed Hv1 [7,19], our results with SH-reagents indicate that this cysteine is in reduced form also in resting granulocytes (Fig. 2b). Redox compounds, e.g. cytoplasmic NADPH [15] or ROS [18], could theoretically affect dimer stability through cys249, but further experiments are required to prove that such changes actually occur and influence the properties of I_{Hv}. Nevertheless, our results with SH-reagents do not indicate a major change in the redox state of this cysteine upon PMA-induced respiratory burst (Fig. 2b). The C-terminal domain of Hv1 forms coiled-coil [19], a structure often involved in interactions between ion channel subunits, and it seems to be involved in Hv1 dimer stabilization [7,8,19]. The role of the largely unstructured N-terminal intracellular domain [7] in dimer formation is less clear. The artificial removal of its intracellular C-terminal domain led to diminished dimer formation by Hv1, a phenomenon that was exacerbated by the concomitant removal of the N-terminal intracellular domain [8]. In our experiments Hv1 appeared prone to cleavage by proteases (Figs. 1c and 3a). How cleavage of intracellular domains could contribute to the changes in I_{Hv} phenotype upon granulocyte activation is not clear, since those changes are largely reversible [15,34]. Nevertheless, the cleavage and/or degradation of the N-terminal domain may still possess a more general regulatory potential in leukocytes, as its overexpression inhibited the proliferation of a premature B-cell lymphoma cell line [35]. In summary, our data do not support the notion that granulocyte activation induces changes in dimer to monomer ratio, as the efficiency of crosslinking was independent of PMA addition (Fig. 2b). Furthermore, based on indirect evidences, the idea that monomer-dimer interconversion occurs during activation of phagocytes was recently challenged by others as well [36].

Hv1 resides mainly in granular membranes in human granulocytes

The heterologously expressed Hv1 was confined to intracellular membranes in HeLa cells in a C-terminus dependent manner. On the other hand, native Hv1 was mainly detected in the plasma membrane and in endosomes of human B-cells [20] (see also Fig. S2a). Our results obtained with subcellular fractionation and confocal imaging concordantly demonstrate that in case of resting human granulocytes Hv1 is mainly located to the membrane of intracellular granules, but its presence at the plasma membrane is also significant (Figs. 3b–c).

The functionally coupled Hv1 and Nox2 are expressed largely independently

Voltage-gated proton channel is viewed as a well-suited tool to support the intense transmembrane electron transport by the phox

during phagocyte respiratory burst [11]. In line with this view, activation of the phox promotes proton channel activity by speeding up its activation, delaying its deactivation and shifting its threshold potential to more negative values [1,37]. Additionally, recent reports demonstrated significant reduction in the ROS producing capability of PMA-activated neutrophils [12,14], bone marrow cells [13] and B-cells [20] from H$_v$1 KO mice. Notably, these cells were devoid of I$_{Hv}$. This strong functional coupling between H$^+$ and e$^-$ transport prompted us to investigate, how the expression and distribution of H$_v$1 and Nox2 are related in human leukocytes. The strong functional coupling of H$_v$1 and phox is nicely reflected in their expression, because a) Nox2 and H$_v$1 display colocalization in different types of phagocytes (Figs. 3a and S2a), b) their expression is induced in parallel during granulocytic differentiation in PLB-985 cells (Fig. 6a) and c) both proteins tend to accumulate in the phagosome membrane during zymosan engulfment (Fig. 4). It has to be emphasized, however, that the accumulation of H$_v$1 in phagosomes and the early and massive induction of H$_v$1 expression during differentiation occur in PLB-985 cells even if functional Nox2 is absent (Figs. 4 and 6a). In analogy with the latter result, resting granulocytes from Nox2 deficient patients display normal I$_{Hv}$ density [1]. Furthermore, we could not detect Nox2 labeling in many of the lymphocytes, which labeled strongly for H$_v$1 (Fig. S2a). The above data confirm that high level H$_v$1 expression does not require the presence of Nox2. Conversely, a massive reduction in H$_v$1 expression does not interfere with the intense expression of phox subunits in PLB-985 cells (Fig. 6b). In this respect it is important that leukocytes from H$_v$1 KO mice express the phox subunits rather normally [12], and exhibit normal Nox2 mediated electron currents [14,38]. Although H$_v$1 and phox are practically independently expressed, the available data indicate that H$_v$1 deficiency leads to restricted phox activity in mouse leukocytes [12–14]. Importantly, no naturally occurring human H$_v$1 deficiency has been reported to date. Chances, however, seem to be low for finding such a case, because, unlike in the mouse, high level H$_v$1 expression is likely required for normal fertility in human [39]. Our results obtained using RNA-interference now demonstrate that severely reduced H$_v$1 expression can become a limiting factor for superoxide production also in granulocytes differentiated from the human leukemia cell line PLB-985 (Fig. 6c).

Is H$_v$1 the only proton channel in neutrophils?

Several lines of evidence indicate that H$_v$1 functions as a proton channel in mouse and human leukocytes. The fact that H$_v$1 is a proton channel does not rule out that another proton channel may exist and might be involved in supporting ROS formation in granulocytes. For many years Nox2 was viewed as a potential candidate to mediate proton current in human granulocytes, especially upon activation of ROS production [16,17]. In this respect it is interesting to note that H$_v$1 deficient mouse leukocytes display significant ROS production [12–14]. Similarly, our PLB-985 clones are capable of intense ROS production even if H$_v$1 expression is severely damaged. These findings may give the impression that H$_v$1 is not the only protein that can attenuate the charge separation by Nox2. Therefore, one has to pose the following questions. Is another proton channel present in neutrophils? If no other proton channel is present, how can one explain the above contradictions? The strongest evidence against an ancillary proton channel was obtained in H$_v$1 deficient mouse neutrophils. These cells display normal electron currents upon activation, but do not show any trace of voltage-gated proton current under resting and PMA-activated conditions [14,38]. This indicates that these cells assemble functional oxidase at the plasma membrane, but neither Nox2 nor another channel seem to conduct protons, at least not in a depolarization-activated fashion. Whether Nox2 or another molecule is capable of conducting protons in a voltage independent manner remains to be tested. How can one explain the significant ROS production in H$_v$1 deficient mouse leukocytes? It is very likely that in a KO system other transporters can partially compensate for the absence of voltage-gated proton channel activity. Furthermore, potassium and chloride channels had been suggested to participate in charge compensation even in normal granulocytes [25]. Whether such mechanisms are upregulated in the absence of H$_v$1 remains to be elucidated. Although some controversy exists [1,16,17], it is likely that similar to the mouse ortholog human Nox2 does not mediate voltage-gated proton current. In line with this assumption, the density of voltage-gated proton current correlates well with H$_v$1 (see above), but not with Nox2 [1] expression among different human leukocyte types and among PLB-985 clones (Fig. 5).

In summary, beside monomers endogenously expressed H$_v$1 forms stable proton channel dimers in resting and activated human granulocytes. The characteristics and expression pattern of H$_v$1 is optimized to support intense phox activity. As the role of ROS production may not be the same in all leukocytes [20,40], the largely independent expression of H$_v$1 and phox components allows fine-tuning of their teamwork.

Materials and Methods

Solutions

For patch-clamp recordings the bath solutions contained (mM): CsCl 1, tetraethylammonium chloride 1, MgCl$_2$ 2, EGTA 1, N-methyl-D-glucamine base 101 and HEPES acid 200 (pH 7.55). The pipette solution contained in (mM): CsCl 1, tetraethylammonium chloride 1, MgCl$_2$ 2, EGTA 1, N-methyl-D-glucamine base 101 and MES acid 200 (pH 6.15). H-medium contained (mM): NaCl 145, KCl 5, MgCl$_2$ 1, CaCl$_2$ 0.8, HEPES 10 and glucose 5 (pH adjusted to 7.4 with NaOH). Disuccinimidyl suberate (DSS), N-ethylmaleimide (NEM), N,N'-(1,3-phenylene)dimaleimide (PDM) were dissolved in DMSO at 250 mM, 400 mM and 10 mM, respectively. Amphotericin B and phorbol-12-myristate-13-acetate (PMA) were first dissolved in DMSO at 80 mg/ml and 5 mM, respectively, then diluted in H-medium to yield stock concentrations of 1 mg/ml and 20 µM, respectively. Phenyl-methanesulfonyl fluoride (PMSF) was dissolved in ethanol at 100 mM.

Cell culture and transfection

All cell lines but PLB-985 X CGD (see below) were purchased from ATCC-LGC (www.lgcstandards-atcc.org) and cultured following the instructions provided by ATCC-LGC with minor modifications, as follow. COS-7 cells were cultured in Dulbecco's modified Eagle's medium (GibcoBRL, Csertex kft, Hungary) supplemented with 10% heat inactivated fetal calf serum (FCS, GIBCO, Invitrogen, www.invitrogen.com), 100 i.u./ml penicillin and 100 µg/ml streptomycin. PLB-985 and Jurkat cells were grown in suspension in complete RPMI 1640 medium supplemented with 10% FCS, 100 i.u./ml penicillin and 100 µg/ml streptomycin. For transfection COS-7 cells were plated in 30 mm plastic tissue culture dishes (Greiner Bio-One, www.greinerbioone.com) and transfected (1 µg plasmid DNA) one day after plating using Lipofectamine 2000 (Invitrogen, www.invitrogen.com). Leukemic (PLB-985 and Jurkat) cells were transfected by electroporation (Amaxa Nucleofector Device, Amaxa Biosystems, www.amaxa.com), using the Cell Line Nucleofector Kit V from (Amaxa Biosystems). For establishing clones from puromycin

(1 μg/ml) resistant cell populations the limiting dilution method was used. For differentiation of PLB-985 and PLB-985 X CGD ([28] generously provided by Mary C. Dinauer, Indianapolis) cells into neutrophil granulocyte like cells, the culture medium was supplemented with 0.5% v/v dimethylformamide (DMFA) with or without reducing the medium's FCS content to 0.5% v/v (to promote differentiation [31]).

Isolation of blood cells and granule fractions

Blood cells were prepared from venous blood drawn from healthy adults after obtaining their informed and written consent. Red blood cells (RBCs) and leukocytes (WBCs) were separated by dextrane sedimentation. To separate mononuclear cells (MCs) from granulocytes (PMNs), WBCs after dextran sedimentation were layered on Ficoll-Paque Plus (GE Healthcare, www.gelifesciences.com) and centrifuged at 400 g for 20 minutes. Remaining RBCs were hemolysed by 30 s exposure to distilled water, followed by reconstitution of the osmolality with equal volume of 1.8% w/v NaCl in distilled water and by centrifugation (400 g, 5 minutes). Pellets containing PMNs or MCs were used to further separate fractions of WBCs by postive or negative selection utilizing fluorochrome or paramagnetically labeled antibodies (MicroBeads) and magnetic separator (VarioMacs) purchased from Miltenyi Biotec (www.miltenyibiotec.com). Eosinophil (CD16-) and Neutrophil (CD16+) fractions of PMNs were separated using CD16 MicroBeads. Monocytes were purified from MCs through positives selection with CD14 MicroBeads. After monocyte depletion of MCs, the remaining lymphocytes could be further dissociated into T-cells and B-cells on a FACSvantage DIVA cell sorter (Becton Dickinson, San Jose, CA) using CD3- or CD19-specific antibodies, respectively (anti-CD3-PE mAb, Beckman Coulter, Fullerton, CA; anti-CD19-FITC mAb, BD Pharmingen, San Diego, CA).

Garnule fractions of human neutrophils were prepared and tested for their identity and purity as described in Ref. [41]. Only preparations that provided the expected antigenicity profile were used. Membrane fractions were boiled for 5 min in reducing Laemmli sample buffer and stored at -70 C until use. The following fractions were separated: azurophil granule (α), specific granule (β$_1$), gelatinase granule (β$_2$) and secretory vesicle along with plasma membrane (γ).

Western blotting

Sample buffers contained 5% v/v β-mercaptoethanol as reducing agent unless otherwise specified. Samples were not heat treated unless otherwise stated. Mononuclear leukocytes were lysed on ice in 2x Laemmli sample buffer. Unless otherwise specified, for lysing granulocytes and PLB cells, 4x Laemmli sample buffer was mixed with equal volume of distilled water (dH$_2$O) supplemented with 5 mM EDTA (250 mM stock in dH$_2$O, pH 7.4 with NaOH) and protease inhibitor cocktail (1 Complete Mini tablet in 10 ml dH$_2$O, Roche Applied Science, www.roche-applied-science.com). When indicated, granulocytes and PLB-985 cells were incubated in nominally calcium and magnesium free media (RPMI 1640 with 5 mM EDTA or PBS) supplemented with diisopropylfluorophosphate (DFP, 1:5000) for 30 min on ice before lysis. DSS crosslinking was performed for 20 min on room temperature. The reaction was quenched by 20 mM TRIS-HCl (pH 8.0). Reactions with NEM (20 mM), PDM (50 μM) or PDM + DSS were carried out on ice for 40 min on ice. PDM crosslinking was quenched with 20 mM NEM. These reagents are lipophil, and were added directly to cells (10^6 cells in 1 ml sterile PBS) in the presence of DFP. After stopping the reactions, cells were pelleted by centrifugation (at 200 g for 3 min)

and lysed in 30 μl 2x Laemmli sample buffer supplemented with 2 mM PMSF. Samples were run on 8 or 10% polyacrylamid gel and blotted onto nitrocellulose membrane. To block non-specific binding sites in Western blot experiments (WB), 5% w/v skimmed milk powder was applied in phosphate buffered saline (PBS, pH 7.4) for 1 hour. After incubating the membranes with the first antibody (rabbit polyclonal or mouse monoclonal) for 1 hour, membranes were washed 5 times in PBS 0.1% v/v Tween20. Horseradish peroxidase labeled anti-rabbit or anti-mouse secondary antibody was added in 1:5000 dilution (in PBS, 0.1% v/v Tween20, 1% w/v skimmed milk powder) for 40 min, followed by washing five times in PBS 0.1% v/v Tween20. Signals were detected on FUJI Super RX films (Fujifilm, www.fujifilm.com) using the enhanced chemiluminescence method (GE Healthcare, ECL^{TM} Western Blotting Analysis System).

Immunofluorescent labeling

In immunofluorescence experiments (IF) cells attached to coverslips were fixed in 4% w/v paraformaldehyde in phosphate buffered saline (PBS, pH 7.4) then rinsed 5 times in PBS and incubated for 10 minutes in PBS containing 100 mM glycine. Coverslips were washed 2 times in PBS and cell permeabilization was carried out in PBS containing 1% w/v bovine serum albumine (BSA) and 0.1% v/v Triton X-100 for 20 min. To block non-specific binding sites (e.g. Fc-receptors of WBCs) 10% v/v pooled human serum (from at least 3 healthy donors, self made), 10% v/v normal goat serum, 10% v/v human Fc-receptor blocking reagent (Miltenyi Biotec) and 1% w/v bovine serum albumin were applied in PBS for 1 h. Coverslips were then incubated with the primary antibody, washed thoroughly 6 times in PBS and incubated with the secondary antibody for 1 hour and finally washed 6 times in PBS again. Coverslips were mounted using Mowiol 4–88 antifade reagent (prepared from polyvinyl alcohol 4–88, glycerol, H$_2$O and TRIS pH 8.5). In IF 5% v/v pooled human serum, 5% v/v normal goat serum, 5% v/v human Fc-receptor blocking reagent and 1% w/v bovine serum albumin were present during the application of antibodies.

Antibodies

To detect human voltage-gated proton channel, affinity purified rabbit polyclonal antibody was used at 2 (WB) or 4–8 (IF) μg/ml. To produce polyclonal anti H$_v$1- antibody (aH$_v$1-N), female white rabbits were immunized with the N-terminal 99 amino acids of H$_v$1 tagged with glutathion-S-transferase. The same peptide construct (covalently bound to Affi-Gel 15 media, Bio-Rad Laboratories, www.bio-rad.com) was used for affinity purification of aH$_v$1-N, after the serum of the immunized rabbit was depleted for anti-glutathion-S-transferase antibodies. As negative control for aH$_v$1-N normal rabbit Ig-G (Santa Cruz Biotechnology, www.sbct.com) was applied at 8 μg/ml. To detect gp91^{phox} with immunofluorescence, supernatant of the mouse monoclonal hybridoma 7D5 [21] was used at 20-time dilution, and purified mouse IgG1 (BD Biosciences Pharmingen, www.bdbiosciences.com) at 2.5 μg/ml served as isotype control. Monoclonal anti-gp91^{phox} antibody (m48ab [42]) was generously provided by Dr Dirk Roos. To detect p47^{phox} or myeloperxoidase, Cell Signaling Technology #4312 or #4162 (www.cellsignal.com) antibody was used, respectively. Anti-p22^{phox} antibody (SC-20781) was purchased from Santa Cruz Biotechnology Inc. (www.scbt.com). Antibodies against gelatinase and CD14 were from Abcam (ab76003 and ab45870, respectively, www.abcam.com). Anti-lactoferrin antibody (L3262) was purchased from Sigma-Aldrich (www.sigmaaldrich.com). For loading control in Western blots anti-protein disulphide isomerase antibody (aPDI) was used

(ab2792, Abcam). Horseradish peroxidase labeled secondary antibodies were from GE Healthcare (for detection with GE Healthcare, ECL^{TM} Western Blotting Analysis System). Alexa Fluor® 488- and Alexa Fluor® 568-labeled secondary antibodies were from Molecular Probes (probes.invitrogen.com).

Confocal laser scanning microscopy and colocalization analysis

Confocal images were collected on an LSM 510 laser scanning confocal unit (Carl Zeiss, www.zeiss.com) with a 63X 1.4 numerical aperture plan Apochromat and a 40X 1.3 numerical aperture plan Neofluar objective (Carl Zeiss). Excitation was with 25 mW argon laser emitting 488 nm, and a 1.0 mW helium/neon laser emitting at 543 nm. Emissions were collected using a 500–530 nm band pass filter to collect Alexa Fluor® 488, and a 560 nm long pass filter to collect Alexa Fluor® 568 emission. Images from optical slices of 1 µm thickness were acquired. LSM software (Carl Zeiss) was used for image acquisition. For analyzing images the ImgaeJ software was applied (Rasband, W. S., U.S. National Institutes of Health, Bethesda, MD, http://rsb.info.nih.gov/ij/). For image processing ImageJ and Pain.Net 3.5 free image editing software (www.paint.net) were used. Analysis of H$_v$1 and Nox2 colocalization was performed only in cells in which at least moderate labeling (two times above background) for both proteins could be detected. For quantification of colocalization the Pearson's coefficient was used [43]. Its value (r) can range from 1 to -1 with r = 1 standing for complete positive correlation and r = -1 for a negative correlation, with r = 0 standing for no correlation in pixel intensities of the two channels. To demonstrate the extent of colocalization in Figs., the colocalization highlighter plugin of the ImageJ software was used. Before applying the plugin, image pairs were corrected for differences in mean signal intensities between the two emission wavelengths. Additionally, pixels with below threshold intensity were excluded from analysis. Unless otherwise stated, threshold was set to 20% of maximal detectable signal intensity. Pixel pairs with intensity ratio between 0.6 and 0.6^{-1} are displayed as colocalizing.

Phagocytosis experiments

Zymosan was opsonized with pooled human serum (from at least 3 healthy donors) by 30-min incubation at 37°C. PMNs (10^8/ml) or 6-day long differentiated PLB-985 cells were allowed to adhere on fibronectin coated glass coverslip for 10 minutes in H-medium. To induce phagocytosis, zymosan was added to phagocytes for 10 min at 37°C to a final concentration of 300 µg/ml.

Detection of superoxide release

To measure extracellular superoxide release, differentiated (for 6–7 days with DMFA) PLB-985 cells were suspended at ~10^6/ml in a 1:1 mixture of Diogenes^{TM} superoxide detection medium (National Diagnostics, www.nationaldiagnostics.com) and H-medium. Aliquots of the suspension (100 µl) were added into wells of white, 96-well plate and prewarmed at 37°C for 15 min. Superoxide induced chemiluminescence was detected at 37°C by a shaking fluoro-luminometer (Ascent Fluoroscan FL, Thermo Scientific, www.thermo.com).

Molecular biology

For cloning of H$_v$1 total RNA from mature dendritic cells was isolated with Trizol reagent (Invitrogen, www.invitrogen.com). cDNA was synthesized from 2.5 µg total RNA using oligo(dt)$_{18}$ primers and RevertAid M-MuLV Reverse Transcriptase (Fer-

mentas, www.fermentas.com) in 20 µl reaction mix. The open reading frame of H$_v$1 was TA cloned into pCDNA3. 1/V5-His-TOPO vector (Invitrogen) with High Fidelity PCR Enzyme (Fermentas) using 1 µl of the first strand as template. The sequence was confirmed by sequencing reactions (Eurofins MWG Operon, www.eurofinsdna.com). For real-time RT-PCR (qPCR) total RNA was isolated as above then treated with DNaseI (Ambion, Austin, TX). Reverse transcription was performed from 100 ng total RNA using Superscript II reverse transcriptase (Invitrogen) and random hexamers (Applied BioSystems, Warrington, United Kingdom) using a standard RT reaction. Amplification reactions were performed in an ABI PRISM 7900 sequence detector (Applied Biosystems) using 40 cycles of 94°C for 12 seconds and 60°C for 1 min. All PCR reactions were done in duplicates with one control reaction not containing RT enzyme. The comparative Ct method was used to quantify the amount of HVCN1 relative to cyclophilin. The following PCR primers and probes were used (5′–3′): forward primer for cyclophilin (NM_021130) ACGGC-GAGCCCTTGG, reverse primer TTTCTGCTGTCTTTGGG-ACCT. Probe was FAM-CGCGTCTCCTTTGAGCTGTTT-GCA-BHQ_1. Taqman gene expression assay for HVCN1 was purchased from Applied Biosystems (Assay ID: Hs00260697_m1). Sequences coding small hairpin RNAs designed to knock down H$_v$1 (HVCN1, transcript variant 1) mRNA level and their minimally changed control sequences were cloned into one of STRIKE^{TM} U6 plasmid vectors (Promega, www.promega.com) either containing green fluorescent protein (Cat.# C3550) or puromycin resistance gene (Cat.# C7900) as selection marker. The following target sequences were used (5′–3′): GAACGG-CAACTCTTAAGGT (si-1), GAACCGGAACTCTTAAGGT (si-1c), GGTGGCCCGGATCATCAAT (si-2), GGTGGCGCG-CATCATCAAT (si-2c).

Patch-clamp measurements

Whole-cell voltage-clamp recordings were performed with an Axoptach-1D patch-clamp amplifier (Axon Instruments, Foster City, CA) equipped with a CV-4-1/100U headstage. Pipettes were pulled from borosilicate glass tubing (type 1B120F-4, World Precision Instruments, Inc., Sarasota, FL) using a P-87 puller (Sutter Instrument Co., CA). After fire polishing, the pipette resistance was 7–13 MΩ when filled with the recording solution. The bath was grounded using an Ag/AgCl pellet. Current signal was low-pass filtered at 100–200 Hz (-3 dB, 8-pole Bessel filter) and sampled at 250–500 Hz. Data acquisition and analysis were performed using pClamp 6 and 8 software (Axon), respectively. To ensure that voltage-gated proton currents were analyzed, reversal potential of the depolarization-activated current was defined using ramp-tail currents, as demonstrated in Fig. S3 and described earlier in detail [15].

Data analysis

Data are presented as mean ± S.E. unless otherwise stated. Statistical analyses were performed using the Statistica software (version 8, Statsoft, Inc., Tulsa, OK, USA). WB and IF experiments were performed at least twice independently unless otherwise stated in the figure legends.

When using transfection reagents, cell labeling kits or other special material the instructions of the manufacturer were rigorously followed. Chemicals were obtained from Sigma-Aldrich unless otherwise specified. All manipulations were performed at room temperature (23–28°C) unless otherwise stated. The studies conformed to the standards set by the Declaration of Helsinki, and the procedures were approved by the ethics committee of Semmelweis University and University of Debrecen.

Supporting Information

Figure S1 A polyclonal antibody selectively recognizes native Hv1. To test the specificity and sensitivity of the antibody, COS-7 cells were transiently transfected with plasmid encoding V5-epitope tagged full length Hv1 (Hv1-V5). (a) Detection of colocalization of anti-V5 and aHv1-N labeling in Hv1-V5 transfected COS-7 cells in immunofluorescence experiments using confocal laser scanning microscopy (Pearson's coefficient is 0.87). The two antibodies label the same cells and cellular structures. Secondary antibodies were labeled with Alexa Fluor® (AF, scale bar, 50 µM). In mock transfected cells only very weak auto fluorescence was detectable (not shown). (b) Result of colocalization analysis performed on pixels with above threshold intensities (see methods). Colocalizing pixels are displayed as white dots in the most right column. (c) Anti-V5 and aHv1-N both detect Hv1-V5 in COS-7 cells transfected with the construct (C+), but not in mock transfected (C-) cells. Only aHv1-N recognizes native Hv1 in human eosinophils (Eo.). Labeling the house keeping enzyme PDI with aPDI served as loading control. The estimated molecular weights (m.w.) of the Hv1 monomer and our Hv1-V5 construct are ~31.6 and ~36.5 kDa, respectively.
Found at: doi:10.1371/journal.pone.0014081.s001 (4.81 MB TIF)

Figure S2 Localization and structure of Hv1 in human leukocytes. (a) Detection of Hv1 (most left column) and Nox2 (middle) in mononuclear cells. Colocalization analysis was performed only in cells in that at least moderate labeling (two times above background) for both proteins could be detected. Above threshold colocalizing pixels are displayed as white dots in the most right column. After correction for differences in mean signal intensities between Hv1 and Nox2 labeling, threshold was set to 20% of maximal detectable intensity. Monocytes displayed strong labeling with aHv1-N, sometimes with strong, colocalizing 7D5 signal. Based on their staining pattern, lymphocytes could be classified into two major groups. Cells in the first group were not stained with either of the two antibodies (not shown), while those in the other group showed strong aHv1-N labeling with strong (lymphocyte 1) to background (lymphocyte 2) 7D5 signal. In lymphocytes aHv1-N labeling often displayed a patchy pattern, which likely arises from endocytotic vesicles (as demonstrated earlier by others [Capasso M. et al., 2010, Nat Immunol 11: 265–272]). Pearson's coefficient for lymphocytes is 0.80±0.02 (n = 4). Scale bars represent 5 µm; Pearson's coefficient for the displayed monocyte is 0.92. (b) Demonstration of Hv1 dimers in human mononuclear leukocytes after cross-liking with DSS in WB after a standard reducing PAGE. Cells were preincubated with DFP (1:5000), and DFP was present during crosslinking.
Found at: doi:10.1371/journal.pone.0014081.s002 (3.80 MB TIF)

Figure S3 Hv1 supports voltage-gated proton current in the human lymphoid leukemia cell line Jurkat. (a) Representative curves from whole cell patch-clamp recordings demonstrate voltage-gated proton current in Jurkat cells transfected with control siRNA, si-2c. Every 15 s, a long-lasting (3 s, A) or short-lasting (0.2 s, B) activating pulse to 80 mV was applied, followed by a rapid voltage ramp to the -90-mV holding potential (C, D). The reversal potential of the voltage- and time-dependent current (inset) was determined by subtracting the two "ramp tail" currents (C–D). (b) Representative curves demonstrate voltage-gated proton current in Jurkat cells transfected with a siRNA (si-2) effective in knocking down Hv1 protein in Hv1-V5 transfected COS-7 cells (not shown). Recordings of transiently transfected Jurkat cells were performed 48–96 h after transfection. Transiently transfected Jurkat cells were identified based on their GFP fluorescence by illuminating the cells

at 488±12 nm using a monochromator equipped 75 watt xenon arc lamp of a monochromator equipped fluorimeter (PTI, South Brunswick, NJ, USA). (c) Voltage protocols used in a and b. (d) Cumulative data of proton current density (amplitude of the time dependent current component normalized to whole cell capacitance) in Jurkat cells transfected transiently with control (si-2c) or effective (si-1 and si-2) siRNA constructs. Si-1-1-C1 is a puromycin selected clone stably expressing si-1. (e) Western blot detection of Hv1 in Jurkat cells. Expression level of the ~36 kDa apparent m.w. protein is reduced in puromycin selected Jurkat cell clone stably expressing si-1, as compared to non-transfected and to puromycin selected, control siRNA (si-1c) transfected Jurkat cells. Labeling with aPDI served as loading control.
Found at: doi:10.1371/journal.pone.0014081.s003 (1.13 MB TIF)

Video S1 Accumulation of Hv1 and Nox2 in the wall of phagosomes in a neutrophil granulocyte. Pseudo color, 3D projection established from a series of 1 µm thin confocal slices taken along the Z axis (perpendicular to the plane of the fibronectin coated coverslip to which the cells are attached). Green denotes aHv1-N labeling (AF 488), while 7D5 (Nox2) labeling is presented in red (AF 568). Only the lower of the two neutrophils in contact displayed labeling with aHv1-N. The double labeled cell engulfed 3 zymosan particles (see also Fig. 4, third column in the manuscript). Zymosan particles can be recognized as labeling-free spherical structures inside the cell. Intense, overlapping clustering of the two signals (yellow) provides better outline of one of the particles. In the analysis only pixels with intensity at least the average intensity observed in experiments performed with control antibodies were included. Projection was performed to the brightest points and pixels are interpolated.
Found at: doi:10.1371/journal.pone.0014081.s004 (0.18 MB MPG)

Video S2 Accumulation of Hv1 and Nox2 in the wall of a phagosome in a differentiated PLB-985 cell. Pseudo color, 3D projection calculated from a series of 1 µm thin confocal slices taken along the Z axis (perpendicular to the plane of the fibronectin coated coverslip to which the cell is attached). Green denotes aHv1-N labeling (AF 488), while 7D5 (Nox2) labeling is presented in red (AF 568). Engulfed zymosan particle can be recognized as labeling-free spherical structure on the cell periphery (see also Fig. 4, fourth column in the manuscript). Intense, overlapping clustering of the two signals can be observed in yellow. In the analysis only pixels with intensity at least two times the average intensity observed in experiments performed with control antibodies were included. Projection was performed to the brightest points, and pixels are interpolated.
Found at: doi:10.1371/journal.pone.0014081.s005 (0.25 MB MPG)

Author Contributions

Conceived and designed the experiments: GLP AO MB IK BR ÁL AR ÉR MG. Performed the experiments: GLP AO MB IK BR ÁL AR MG. Analyzed the data: GLP AO MB IK ÁL MG. Contributed reagents/materials/analysis tools: GLP ÁL ÉR MG. Wrote the paper: GLP AO MB ÁL MG.

References

1. DeCoursey TE (2003) Voltage-gated proton channels and other proton transfer pathways. Physiol Rev 83: 475–579.
2. Sasaki M, Takagi M, Okamura Y (2006) A Voltage Sensor-Domain Protein is a Voltage-Gated Proton Channel. Science 312: 589–592.
3. Ramsey IS, Moran MM, Chong JA, Clapham DE (2006) A voltage-gated proton-selective channel lacking the pore domain. Nature 440: 1213–1216.
4. Musset B, Cherny VV, Morgan D, Okamura Y, Ramsey IS, et al. (2008) Detailed comparison of expressed and native voltage-gated proton channel currents. J Physiol 586: 2477–2486.
5. Lee SY, Letts JA, Mackinnon R (2009) Functional reconstitution of purified human Hv1 H+ channels. J Mol Biol 387: 1055–1060.
6. Tombola F, Ulbrich MH, Isacoff EY (2008) The voltage-gated proton channel Hv1 has two pores, each controlled by one voltage sensor. Neuron 58: 546–556.
7. Lee SY, Letts JA, Mackinnon R (2008) Dimeric subunit stoichiometry of the human voltage-dependent proton channel Hv1. Proc Natl Acad Sci U S A 105: 7692–7695.
8. Koch HP, Kurokawa T, Okochi Y, Sasaki M, Okamura Y, et al. (2008) Multimeric nature of voltage-gated proton channels. Proc Natl Acad Sci U S A 105: 9111–9116.
9. DeCoursey TE (2008) Voltage-gated proton channels: what's next? J Physiol 586: 5305–5324.
10. Shepherd VL (1986) The role of the respiratory burst of phagocytes in host defense. Semin Respir Infect 1: 99–106.
11. Murphy R, DeCoursey TE (2006) Charge compensation during the phagocyte respiratory burst. Biochim Biophys Acta 1757: 996–1011.
12. Okochi Y, Sasaki M, Iwasaki H, Okamura Y (2009) Voltage-gated proton channel is expressed on phagosomes. Biochem Biophys Res Commun 382: 274–279.
13. Ramsey IS, Ruchti E, Kaczmarek JS, Clapham DE (2009) Hv1 proton channels are required for high-level NADPH oxidase-dependent superoxide production during the phagocyte respiratory burst. Proc Natl Acad Sci U S A 106: 7642–7647.
14. El Chemaly A, Okochi Y, Sasaki M, Arnaudeau S, Okamura Y, et al. (2010) VSOP/Hv1 proton channels sustain calcium entry, neutrophil migration, and superoxide production by limiting cell depolarization and acidification. J Exp Med 207: 129–2.
15. Petheo GL, Maturana A, Spat A, Demaurex N (2003) Interactions between electron and proton currents in excised patches from human eosinophils. J Gen Physiol 122: 713–726.
16. Henderson LM, Meech RW (2002) Proton Conduction through gp91(phox). J Gen Physiol 120: 759–765.
17. Maturana A, Krause KH, Demaurex N (2002) NOX Family NADPH Oxidases: Do They Have Built-in Proton Channels? J Gen Physiol 120: 781–786.
18. Annunziato L, Pannaccione A, Cataldi M, Secondo A, Castaldo P, et al. (2002) Modulation of ion channels by reactive oxygen and nitrogen species: a pathophysiological role in brain aging? Neurobiol Aging 23: 819–834.
19. Li SJ, Zhao Q, Zhou Q, Unno H, Zhai Y, et al. (2010) The role and structure of the carboxyl-terminal domain of the human voltage-gated proton channel Hv1. J Biol Chem.
20. Capasso M, Bhamrah MK, Henley T, Boyd RS, Langlais C, et al. (2010) HVCN1 modulates BCR signal strength via regulation of BCR-dependent generation of reactive oxygen species. Nat Immunol 11: 265–272.
21. Nakamura M, Murakami M, Koga T, Tanaka Y, Minakami S (1987) Monoclonal antibody 7D5 raised to cytochrome b558 of human neutrophils: immunocytochemical detection of the antigen in peripheral phagocytes of normal subjects, patients with chronic granulomatous disease, and their carrier mothers. Blood 69: 1404–1408.
22. Borregaard N, Cowland JB (1997) Granules of the human neutrophilic polymorphonuclear leukocyte. Blood 89: 3503–3521.
23. Ginsel LA, Onderwater JJ, Fransen JA, Verhoeven AJ, Roos D (1990) Localization of the low-Mr subunit of cytochrome b558 in human blood phagocytes by immunoelectron microscopy. Blood 76: 2105–2116.
24. Tsang JL, Parodo JC, Marshall JC (2010) Regulation of apoptosis and priming of neutrophil oxidative burst by diisopropyl fluorophosphate. J Inflamm (Lond) 7: 32.
25. Segal AW (2005) How neutrophils kill microbes. Annu Rev Immunol 23: 197–223.
26. van Manen HJ, Uzunbajakava N, van Bruggen R, Roos D, Otto C (2003) Resonance Raman imaging of the NADPH oxidase subunit cytochrome b558 in single neutrophilic granulocytes. J Am Chem Soc 125: 12112–12113.
27. van Bruggen R, Anthony E, Fernandez-Borja M, Roos D (2004) Continuous translocation of Rac2 and the NADPH oxidase component p67(phox) during phagocytosis. J Biol Chem 279: 9097–9102.
28. Zhen L, King AA, Xiao Y, Chanock SJ, Orkin SH, et al. (1993) Gene targeting of X chromosome-linked chronic granulomatous disease locus in a human myeloid leukemia cell line and rescue by expression of recombinant gp91phox. Proc Natl Acad Sci U S A 90: 9832–9836.
29. Qu AY, Nanda A, Curnutte JT, Grinstein S (1994) Development of a H(+)-selective conductance during granulocytic differentiation of HL-60 cells. Am J Physiol 266: C1263–C1270.
30. Drexler HG, Dirks WG, Matsuo Y, MacLeod RA (2003) False leukemia-lymphoma cell lines: an update on over 500 cell lines. Leukemia 17: 416–426.
31. Pedruzzi E, Fay M, Elbim C, Gaudry M, Gougerot-Pocidalo MA (2002) Differentiation of PLB-985 myeloid cells into mature neutrophils, shown by degranulation of terminally differentiated compartments in response to N-formyl peptide and priming of superoxide anion production by granulocyte-macrophage colony-stimulating factor. Br J Haematol 117: 719–726.
32. Hladky SB, Haydon DA (1972) Ion transfer across lipid membranes in the presence of gramicidin A. I. Studies of the unit conductance channel. Biochim Biophys Acta 274: 294–312.
33. Tombola F, Ulbrich MH, Kohout SC, Isacoff EY (2010) The opening of the two pores of the Hv1 voltage-gated proton channel is tuned by cooperativity. Nat Struct Mol Biol 17: 44–50.
34. DeCoursey TE, Cherny VV, Zhou W, Thomas LL (2000) Simultaneous activation of NADPH oxidase-related proton and electron currents in human neutrophils. Proc Natl Acad Sci U S A 97: 6885–6889.
35. Suenaga T, Arase H, Yamasaki S, Kohno M, Yokosuka T, et al. (2007) Cloning of B cell-specific membrane tetraspanning molecule BTS possessing B cell proliferation-inhibitory function. Eur J Immunol 37: 3197–3207.
36. Musset B, Smith SM, Rajan S, Cherny VV, Sujai S, et al. (2010) Zinc Inhibition of Monomeric and Dimeric Proton Channels Suggests Cooperative Gating. J Physiol.
37. Banfi B, Schrenzel J, Nusse O, Lew DP, Ligeti E, et al. (1999) A novel H(+) conductance in eosinophils: unique characteristics and absence in chronic granulomatous disease. J Exp Med 190: 183–194.
38. Morgan D, Capasso M, Musset B, Cherny VV, Rios E, et al. (2009) Voltage-gated proton channels maintain pH in human neutrophils during phagocytosis. Proc Natl Acad Sci U S A 106: 18022–18027.
39. Lishko PV, Botchkina IL, Fedorenko A, Kirichok Y (2010) Acid extrusion from human spermatozoa is mediated by flagellar voltage-gated proton channel. Cell 140: 327–337.
40. Fisher AB (2009) Redox signaling across cell membranes. Antioxid Redox Signal 11: 1349–1356.
41. Kjeldsen L, Bjerrum OW, Askaa J, Borregaard N (1992) Subcellular localization and release of human neutrophil gelatinase, confirming the existence of separate gelatinase-containing granules. Biochem J 287: 603–610.
42. Burritt JB, Fritel GN, Dahan I, Pick E, Roos D, et al. (2000) Epitope identification for human neutrophil flavocytochrome b monoclonals 48 and 449. Eur J Haematol 65: 407–413.
43. Bolte S, Cordelieres FP (2006) A guided tour into subcellular colocalization analysis in light microscopy. J Microsc 224: 213–232.